

Supporting Information

ESIPT-Active 8-Hydroxyquinoline Chemosensor for Highly Selective Detection of Diethyl Chlorophosphate and Molecular Logic Gate Applications

Aastha Palta^a, Gulshan Kumar^b, Kamaldeep Paul^c and Vijay Luxami^{c*}

^aUniversity Centre for Research and Development, Chandigarh University, Mohali-140413, India

^bDepartment of Chemistry, Banasthali University, Banasthali Newai, 304022 Rajasthan, India

^cDepartment of Chemistry and Biochemistry, Thapar Institute of Engineering and Technology, Patiala-147001, India

Email: vluxami@thapar.edu

Table of Contents:

Figure S1: ^1H NMR spectrum of **HQHBI**.

Figure S2: ^{13}C NMR spectrum of **HQHBI**.

Figure S3: HRMS spectrum of **HQHBI**.

Figure S4: Comparison of calculated absorption spectra at different functional with experimental absorption spectra peak.

Figure S5: Plot for the determination of lowest detection limit of **HQHBI** ($20\ \mu\text{M}$) with DCP in H_2O : CH_3CN , 1:1 [v/v].

Figure S6: Benesi-Hildebrand plot for determination of binding constant of **HQHBI** ($20\ \mu\text{M}$) with DCP in H_2O : CH_3CN , 1:1 [v/v].

Figure S7: Job's Plot for **HQHBI** ($20\ \mu\text{M}$) binding with DCP ($20\ \mu\text{M}$) in H_2O : CH_3CN , 1:1 [v/v].

Table S1: Comparison with previously reported DCP sensors.

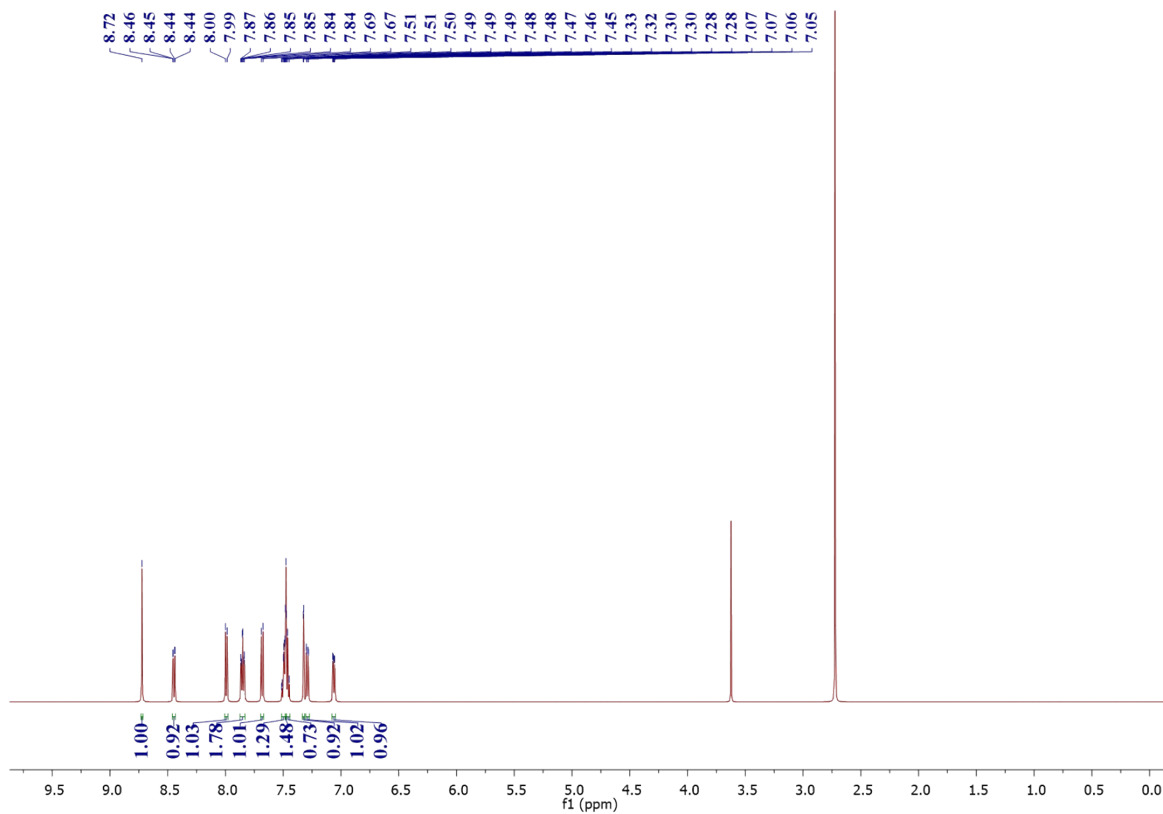


Figure S1: ^1H NMR spectrum of HQHBI.

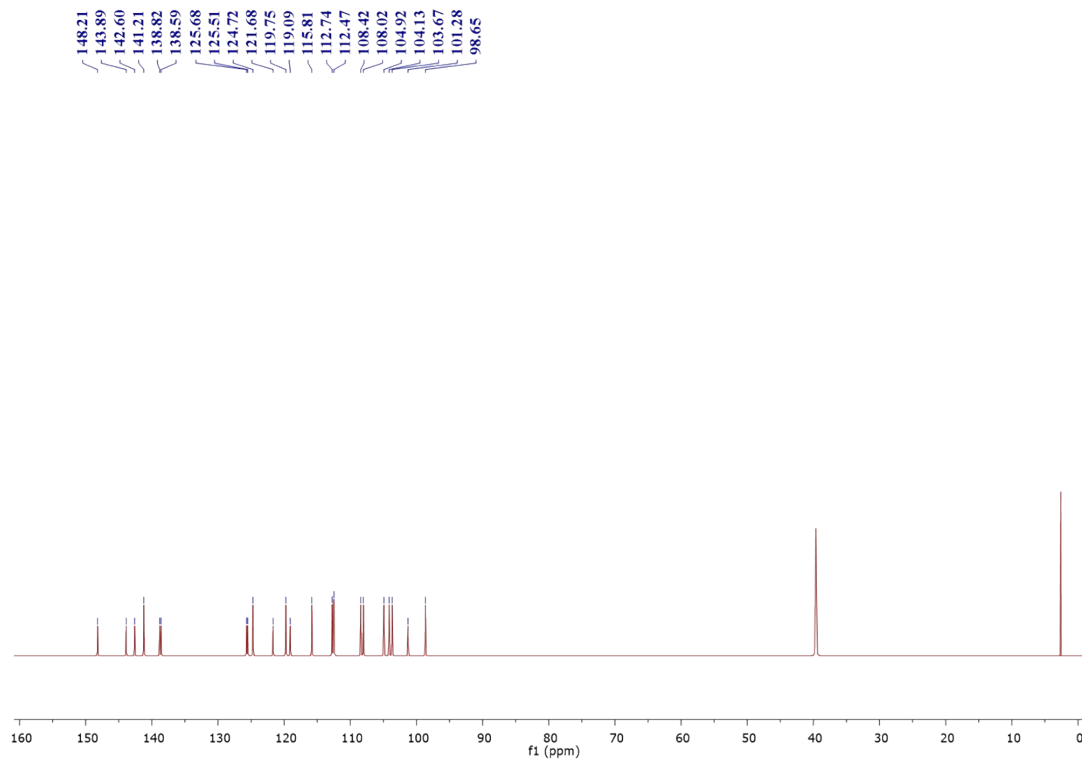


Figure S2: ^{13}C NMR spectrum of HQHBI.

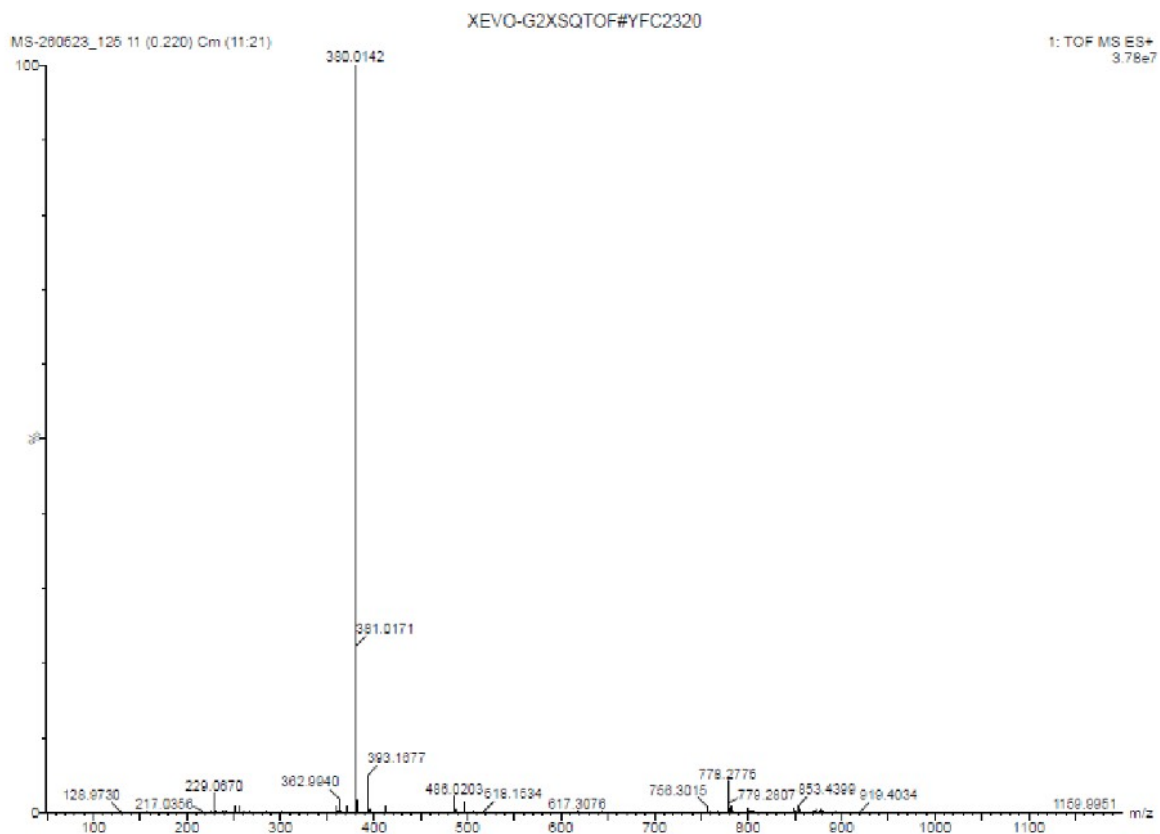


Figure S3: HRMS spectrum of HQHBI.

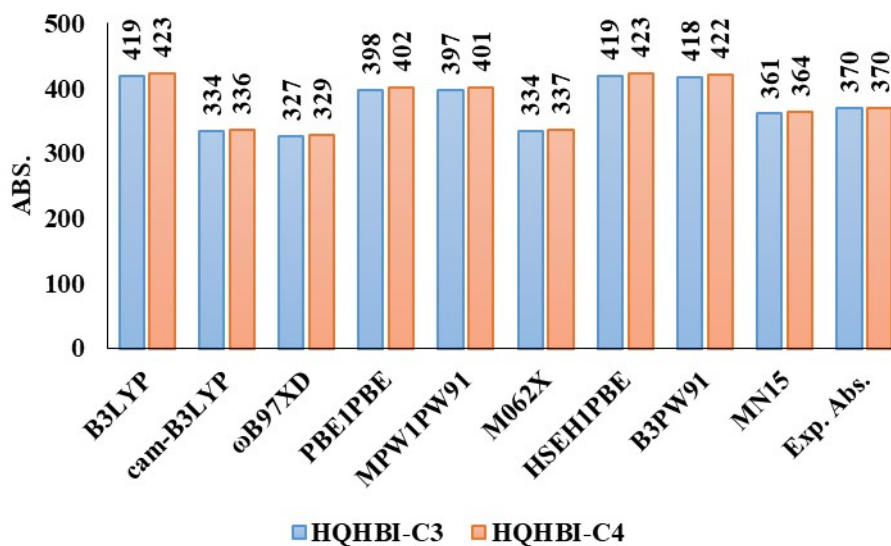


Figure S4: Comparison of calculated absorption spectra at different functional with experimental absorption spectra peak.

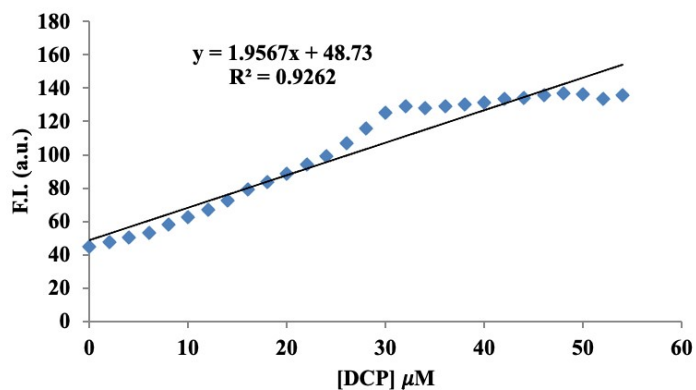


Figure S5: Plot for the determination of lowest detection limit of **HQHBI** ($20\ \mu\text{M}$) with DCP in H_2O : CH_3CN , 1:1 [v/v].

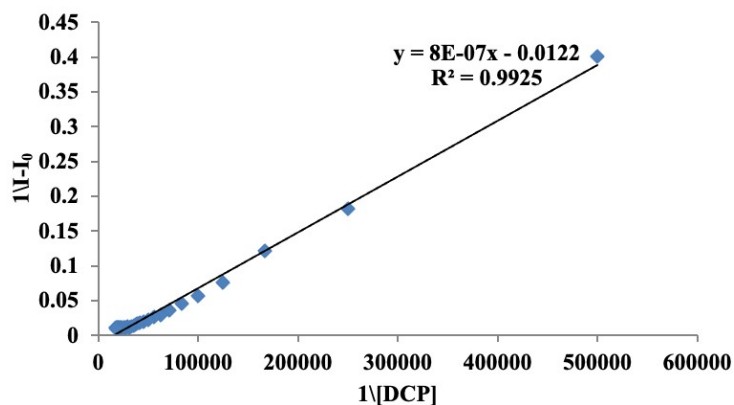


Figure S6: Benesi-Hildebrand plot for determination of binding constant of **HQHBI** ($20\ \mu\text{M}$) with DCP in H_2O : CH_3CN , 1:1 [v/v].

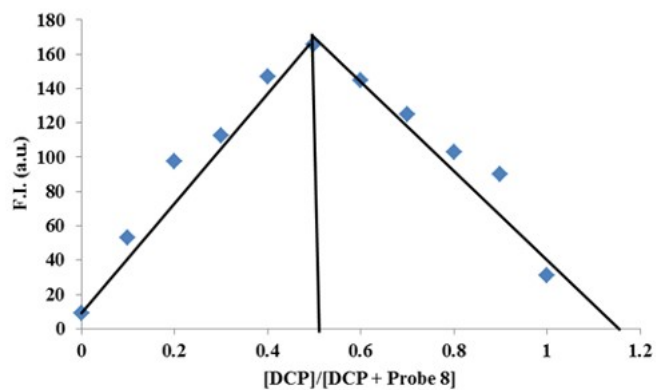
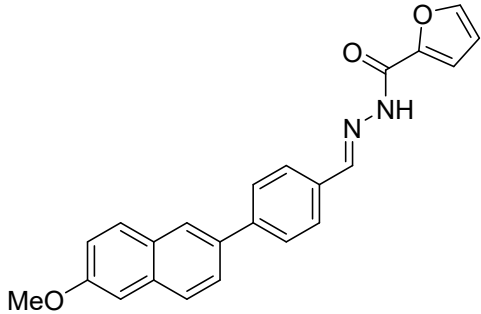
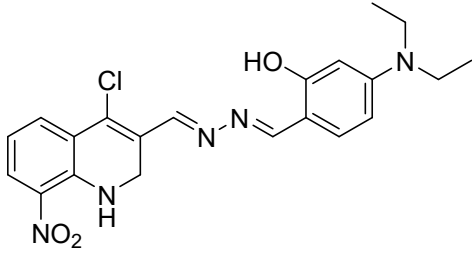
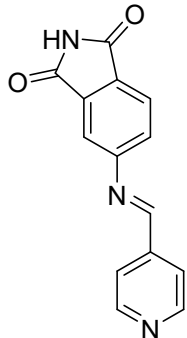
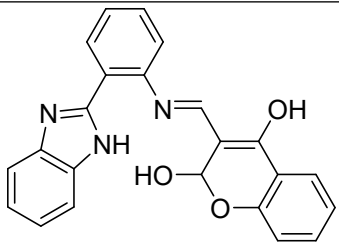
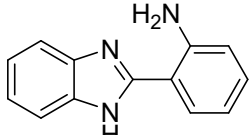
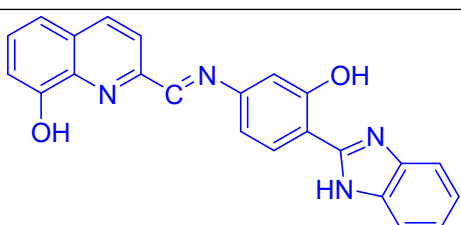


Figure S7: Job's Plot for **HQHBI** ($20\ \mu\text{M}$) binding with DCP ($20\ \mu\text{M}$) in H_2O : CH_3CN , 1:1 [v/v].

Table S1: Comparison with previously reported DCP sensors.

S. No.:	Structure	Solvent	Selectivity	Limit of detection	References
1		CH ₃ CN	DCP	12.2 nM	1
2		DMF	DCP	1.5 μM	2
3		CH ₃ CN	DCP	24 nM	3
4		CH ₃ CN	DCP	6.6 μM	4
5		CH ₃ CN	DCP	20.9 μM	5
6		H ₂ O: CH ₃ CN, 1:1 [v/v]	DCP	0.15 μM	This Work

1. S. Banerjee, P. Ghosh, A. Karak, D. Banik, and A. K. Mahapatra, A chemodosimetric chemosensor for the ratiometric detection of nerve agent-mimic DCP in solution and vapor phases, *Anal. Methods*, 2025, **17**, 432-439.
2. S.S.Ramasamy, K. Adhigaman, V. Nandakumar, A. Muralidharan, S. Ramasamy, and S. Thangaraj, Design and synthesis of 8-nitroquinoline azine D- π -A module chemosensors: Fluorogenic onsite detection of sarin gas mimic-DCP, *Talanta Open*, 2025, **12**, 100508.
3. X. Wen, T. Jiang, T. Liu, B. Zhao, X. Xu, H. Jeong, C. Fan, Y. Sun, J. Yoon, and Z. Lu, Schiff base-based turn-on fluorescent probe for rapid on-site detection of nerve agent simulants in solution and vapor, *Microchem. J.*, 2026, **224**, 117473.
4. N. Tohora, C. Debnath, S. Ahamed, J. Chourasia, M. Mahato, S. Ali, S. Lama, S. Pradhan, and S. K. Das, An efficient ESIPT-based ratio-/fluorimetric probe for rapid and sensitive detection of the sarin surrogate diethylchlorophosphate in solution and vapor phases, *Anal. Methods*, 2025, **17**, 2067-2075.
5. A. D. Jaiswal, J. Chourasia, S. Ahamed, N. Tohora, S. Lama, M. Mahato, U. Darnal, S. Ghanta, and S. K. Das, Decrypting the mechanistic aspect of a fluorochromic diethylchlorophosphate sensitive benzimidazole based probe: A combined spectroscopic and theoretical investigation, *Microchem. J.*, 2025, **212**, 113421.